Theory of supercurrent transport in SIsFS Josephson junctions

S. V. Bakurskiy,[1,2,3] N. V. Klenov,[2] I. I. Soloviev,[1] M. Yu. Kupriyanov,[1] and A. A. Golubov[3]

[1]*Skobeltsyn Institute of Nuclear Physics, Lomonosov Moscow State University, Leninskie gory, Moscow 119991, Russian Federation*

[2]*Faculty of Physics, Lomonosov Moscow State University, Leninskie gory, Moscow 119992, Russian Federation*

[3]*Faculty of Science and Technology and MESA+ Institute for Nanotechnology, University of Twente, 7500 AE Enschede, The Netherlands*

(Received 14 June 2013; revised manuscript received 20 September 2013; published 31 October 2013)

We present the results of a theoretical study of current-phase relations (CPRs) $J_S(\varphi)$ in Josephson junctions of SIsFS type, where S is a bulk superconductor and IsF is a complex weak link consisting of a superconducting film s, a metallic ferromagnet F, and an insulating barrier I. At temperatures close to critical, $T \lesssim T_C$, calculations are performed analytically in the frame of the Ginsburg-Landau equations. At low temperatures a numerical method is developed to solve self-consistently the Usadel equations in the structure. We demonstrate that SIsFS junctions have several distinct regimes of supercurrent transport and we examine spatial distributions of the pair potential across the structure in different regimes. We study the crossover between these regimes, which is caused by shifting the location of a weak link from the tunnel barrier I to the F layer. We show that strong deviations of the CPR from sinusoidal shape occur even in the vicinity of T_C, and these deviations are strongest in the crossover regime. We demonstrate the existence of temperature-induced crossover between 0 and π states in the contact and show that the smoothness of this transition strongly depends on the CPR shape.

DOI: 10.1103/PhysRevB.88.144519 PACS number(s): 74.45.+c, 74.50.+r, 74.78.Fk, 85.25.Cp

I. INTRODUCTION

Josephson structures with a ferromagnetic layer became a very active field of research because of the interplay between superconducting and magnetic order in a ferromagnet, leading to a variety of new effects including the realization of a π state with phase difference π in the ground state of a junction, as well as long-range Josephson coupling due to generation of an odd-frequency triplet order parameter.[1–3]

Further interest in Josephson junctions with a magnetic barrier is due to emerging possibilities for their practical use as elements of a superconducting memory,[4–12] on-chip π phase shifters for self-biasing various electronic quantum and classical circuits,[13–16] and φ batteries, structures having in the ground state a phase difference $\varphi_g = \varphi$ $(0 < |\varphi| < \pi)$ between superconducting electrodes.[17–25] In standard experimental implementations superconductor-ferromagnet-superconductor (SFS) Josephson contacts are sandwich-type structures.[26,27] The characteristic voltage $V_C = J_C R_N$ (J_C is the critical current of the junction and R_N is the resistance in the normal state) of these SFS devices is typically quite low, which limits their practical applications. In SIFS structures[28–32] containing an additional insulating tunnel barrier I, the $J_C R_N$ product in the 0 state is increased,[9] but in the π state V_C is still too small[33,34] due to strong suppression of the superconducting correlations in the ferromagnetic layer.

Recently, a different type of magnetic Josepshon junction was realized experimentally, containing two superconducting layers with IsF a complex weak link consisting of a superconducting film s, a metallic ferromagnet F, and an insulating barrier I.[9–12] This structure represents a connection of an SIs tunnel junction and an sFS contact in series. Properties of SIsFS structures are controlled by the thickness of the s layer d_s and by the relation between the critical currents J_{CSIs} and J_{CsFS} of their SIs and sFS parts, respectively. If the thickness of the s layer d_s is much larger than its coherence length ξ_s and $J_{CSIs} \ll J_{CsFS}$, then the characteristic voltage of an SIsFS device is determined by its SIs part and may reach its maximum corresponding to a standard SIS junction. At the same time, the phase difference φ in the ground state of an SIsFS junction is controlled by its sFS part. As a result, both 0 and π states can be achieved depending on the thickness of the F layer. This opens the possibility of realizing controllable π junctions having a large $J_C R_N$ product. At the same time, when placed in an external magnetic field H_{ext}, the SIsFS structure behaves as a single junction, since d_s is typically too thin to screen H_{ext}. This provides the possibility of switching J_C by an external field.

The purpose of this paper is to develop a microscopic theory providing the dependence of the characteristic voltage on temperature T, exchange energy H in the ferromagnet, transport properties of FS and sF interfaces, and the thicknesses of the s and F layers. Special attention will be given to determining the current-phase relation (CPR) between the supercurrent J_S and the phase difference φ across the structure.

II. MODEL OF SISFS JOSEPHSON DEVICE

We consider the multilayered structure presented in Fig. 1(a). It consists of two superconducting electrodes separated by a complex interlayer including a tunnel barrier I and intermediate superconducting s and ferromagnetic F films. We assume that the conditions of the dirty limit are fulfilled for all materials in the structure. In order to simplify the problem, we also assume that all superconducting films are identical and can be described by a single critical temperature T_C and coherence length ξ_S. Transport properties of both sF and FS interfaces are also assumed identical and are characterized by the interface parameters

$$\gamma = \frac{\rho_S \xi_S}{\rho_F \xi_F}, \quad \gamma_B = \frac{R_{BF} \mathcal{A}_B}{\rho_F \xi_F}. \tag{1}$$

Here R_{BF} and $\mathcal{A}_B$ are the resistance and area of the sF and FS interfaces, ξ_S and ξ_F are the decay lengths of S and F materials, and ρ_S and ρ_F are their resistivities.

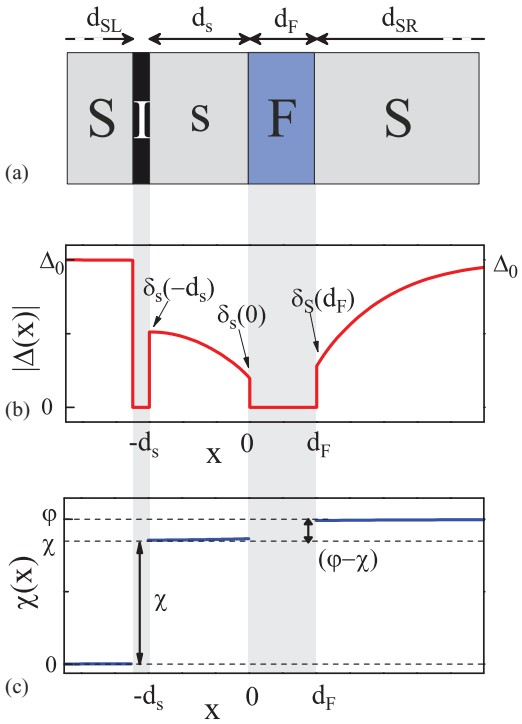

FIG. 1. (Color online) (a) Schematic design of SIsFS Josephson junction. (b),(c) Typical distributions of amplitude $|\Delta(x)|$ and phase difference $\chi(x)$ of the pair potential along the structure.

Under the above conditions the problem of calculation of the critical current in the SIsFS structure reduces to solution of the set of Usadel equations.[35] For the S layers these equations have the forms[1–3]

$$\frac{\xi_S^2}{\Omega G_m}\frac{d}{dx}\left(G_m^2\frac{d}{dx}\Phi_m\right)-\Phi_m=-\Delta_m, \qquad G_m=\frac{\Omega}{\sqrt{\Omega^2+\Phi_m\Phi_m^*}}, \tag{2}$$

$$\Delta_m\ln\frac{T}{T_C}+\frac{T}{T_C}\sum_{\omega=-\infty}^{\infty}\left(\frac{\Delta_m}{|\Omega|}-\frac{\Phi_m G_m}{\Omega}\right)=0, \tag{3}$$

where $m=S$ for $x\leqslant -d_s$ and $x\geqslant d_F$; $m=s$ in the interval $-d_s\leqslant x\leqslant 0$. In the F film ($0\leqslant x\leqslant d_F$) the equation is

$$\xi_F^2\frac{d}{dx}\left(G_F^2\frac{d}{dx}\Phi_F\right)-\widetilde{\Omega}\Phi_F G_F=0. \tag{4}$$

Here $\Omega=T(2n+1)/T_C$ are Matsubara frequencies normalized to πT_C, $\widetilde{\Omega}=\Omega+iH/\pi T_C$, $G_F=\widetilde{\Omega}/(\widetilde{\Omega}^2+\Phi_{F,\omega}\Phi^*_{F,-\omega})^{1/2}$, H is the exchange energy, $\xi^2_{S,F}=(D_{S,F}/2\pi T_C)$, and $D_{S,F}$ are the diffusion coefficients in the S and F metals, respectively. The pair potential Δ_m and the Usadel functions Φ_m and Φ_F in (2)–(4) are also normalized to πT_C. To write Eqs. (2)–(4), we have chosen the x axis in the direction perpendicular to the SI, FS, and sF interfaces and put the origin at the sF interface. Equations (2)–(4) must be supplemented by the boundary conditions.[36] At $x=-d_s$ they can be written as

$$G_S^2\frac{d}{dx}\Phi_S=G_s^2\frac{d}{dx}\Phi_s, \quad \gamma_{BI}\xi_S G_s\frac{d}{dx}\Phi_s=-G_S(\Phi_S-\Phi_s), \tag{5}$$

where $\gamma_{BI}=R_{BI}\mathcal{A}_B/\rho_S\xi_S$, and R_{BI} and $\mathcal{A}_B$ are the resistance and area of the SI interface. At $x=0$ the boundary conditions are

$$\frac{\xi_S}{\Omega}G_s^2\frac{d}{dx}\Phi_s=\gamma\frac{\xi_F}{\widetilde{\Omega}}G_F^2\frac{d}{dx}\Phi_F, \qquad \gamma_B\xi_F G_F\frac{d}{dx}\Phi_F=-G_s\left(\frac{\widetilde{\Omega}}{\Omega}\Phi_s-\Phi_F\right) \tag{6}$$

and at $x=d_F$ they have the form

$$\frac{\xi_S}{\Omega}G_S^2\frac{d}{dx}\Phi_S=\gamma\frac{\xi_F}{\widetilde{\Omega}}G_S^2\frac{d}{dx}\Phi_F, \qquad \gamma_B\xi_F G_F\frac{d}{dx}\Phi_F=G_S\left(\frac{\widetilde{\Omega}}{\Omega}\Phi_S-\Phi_F\right). \tag{7}$$

Far from the interfaces the solution should cross over to a uniform current-carrying superconducting state[37–39]

$$\Phi_S(\mp\infty)=\Phi_\infty\exp\{i(\chi(\mp\infty)-ux/\xi_S)\}, \tag{8}$$

$$\Delta_S(\mp\infty)=\Delta_0\exp\{i(\chi(\mp\infty)-ux/\xi_S)\}, \tag{9}$$

$$\Phi_\infty=\frac{\Delta_0}{1+u^2/\sqrt{\Omega^2+|\Phi_S|^2}}, \tag{10}$$

resulting in an order parameter phase difference across the structure equal to

$$\varphi=\varphi(\infty)-2ux/\xi_S, \quad \varphi(\infty)=\chi(\infty)-\chi(-\infty). \tag{11}$$

Here $\varphi(\infty)$ is the asymptotic phase difference across the junction, Δ_0 is the modulus of order parameters far from the boundaries of the structure at a given temperature, $u=2mv_s\xi_S$, m is the electron mass, and v_s is the superfluid velocity. Note that since the boundary conditions (5) and (6) include the Matsubara frequency Ω, the phases of the functions Φ_S depend on Ω and are different from the phases of the pair potential Δ_S at the FS interfaces $\chi(d_F)$ and $\chi(0)$. Therefore it is the value $\varphi(\infty)$ rather than $\varphi=\chi(d_F)-\chi(0)$ that can be measured experimentally by using a scheme compensating the linear in x part in Eq. (11).

The boundary problem (2)–(11) can be solved numerically making use of (8) and (10). The accuracy of the calculations can be monitored by the equality of the currents J_S

$$\frac{2eJ_S(\varphi)}{\pi T\mathcal{A}_B}=\sum_{\omega=-\infty}^{\infty}\frac{iG_{m,\omega}^2}{\rho_m\widetilde{\Omega}^2}\left[\Phi_{m,\omega}\frac{\partial\Phi^*_{m,-\omega}}{\partial x}-\Phi^*_{m,-\omega}\frac{\partial\Phi_{m,\omega}}{\partial x}\right] \tag{12}$$

calculated at the SI and FS interfaces and in the electrodes.

In the further analysis carried out below we limit ourselves to the consideration of the most relevant case of a low-transparency tunnel barrier at the SI interface,

$$\gamma_{BI}\gg 1. \tag{13}$$

In this approximation, the junction resistance R_N is fully determined by the barrier resistance R_{BI}. Furthermore the current flowing through the electrodes can lead to the suppression of superconductivity only in the vicinity of sF and FS interfaces. That means, up to terms of the order of γ_{BI}^{-1} we can neglect the effects of suppression of superconductivity in the region

$x \leqslant -d_s$ and write the solution in the form

$$\Phi_S(x) = \Delta_S(x) = \Delta_0. \tag{14}$$

Here without any loss of generality we put $\chi(-\infty) = \chi(-d_s - 0) = 0$ [see Fig. 1(c)].

Substitution of (14) into the boundary conditions (5) gives

$$\gamma_{BI}\xi_S G_s \frac{d}{dx}\Phi_s = -\frac{\Omega}{\sqrt{\Omega^2 + \Delta_0^2}}(\Delta_0 - \Phi_s). \tag{15}$$

Further simplifications are possible in several limiting cases.

III. THE HIGH-TEMPERATURE LIMIT $T \approx T_C$

In the vicinity of the critical temperature the Usadel equations in the F layer can be linearized. Writing down their solution in analytical form and using the boundary conditions (6) and (7) on sF and FS interfaces we can reduce the problem to the solution of the Ginzburg-Landau (GL) equations in the s and S layers. We limit our analysis by considering the most interesting case when the following condition is fulfilled:

$$\Gamma_{BI} = \frac{\gamma_{BI}\xi_S}{\xi_S(T)} \gg 1, \tag{16}$$

and when there is strong suppression of superconductivity in the vicinity of the sF and FS interfaces. The latter takes place if the parameter Γ,

$$\Gamma = \frac{\gamma\xi_S(T)}{\xi_S}, \quad \xi_S(T) = \frac{\pi\xi_S}{2\sqrt{1 - T/T_C}}, \tag{17}$$

satisfies the conditions

$$\Gamma p \gg 1, \quad \Gamma q \gg 1. \tag{18}$$

Here

$$p^{-1} = \frac{8}{\pi^2}\mathrm{Re}\sum_{\omega=0}^{\infty}\frac{1}{\Omega^2\sqrt{\widetilde{\Omega}}\coth\frac{d_F\sqrt{\widetilde{\Omega}}}{2\xi_F}}, \tag{19}$$

$$q^{-1} = \frac{8}{\pi^2}\mathrm{Re}\sum_{\omega=0}^{\infty}\frac{1}{\Omega^2\sqrt{\widetilde{\Omega}}\tanh\frac{d_F\sqrt{\widetilde{\Omega}}}{2\xi_F}}. \tag{20}$$

Note that in the limit $h = H/\pi T_C \gg 1$ and $d_F \gg \sqrt{2/h}\xi_F$ the sums in (19) and (20) can be evaluated analytically, resulting in

$$\beta = \frac{p-q}{p+q} = \sqrt{8}\sin\left(\frac{d_F}{\xi_F}\sqrt{\frac{h}{2}} + \frac{3\pi}{4}\right)\exp\left(-\frac{d_F}{\xi_F}\sqrt{\frac{h}{2}}\right), \tag{21}$$

$$p + q = 2\sqrt{2h}(T/T_C)^2, \quad pq = 2h(T/T_C)^4. \tag{22}$$

In general, the phases of the order parameters in the s and S films are functions of the coordinate x. In the considered approximation the terms that take into account the coordinate dependence of the phases are proportional to the small parameters $(\Gamma q)^{-1}$ and $(\Gamma p)^{-1}$ and therefore provide small corrections to the current. For this reason, in the first approximation we can assume that the phases in superconducting electrodes are constants independent of x. In the further analysis we denote the phases at the s film by χ and at the right S electrode by φ [see Fig. 1(c)].

The details of the calculations are summarized in the Appendix. These calculations show that the considered SIsFS junction has two modes of operation depending on the relation between the s layer thickness d_s and the critical thickness $d_{sc} = (\pi/2)\xi_S(T)$. For d_s larger than d_{sc}, the s film keeps its intrinsic superconducting properties (mode 1), while for $d_s \leqslant d_{sc}$ superconductivity in the s film exists only due to the proximity effect with the bulk S electrodes (mode 2).

A. Mode 1: SIs + sFS junction $d_s \geqslant d_{sc}$

We begin our analysis with the regime when the intermediate s layer is intrinsically superconducting. In this case it follows from the solution of the GL equations that the supercurrent flowing across the SIs, sF, and FS interfaces [$J(-d_s)$, $J(0)$, and $J(d_F)$, respectively] can be represented in the form (see the Appendix)

$$\frac{J_S(-d_s)}{J_G} = \frac{\delta_s(-d_s)}{\Gamma_{BI}\Delta_0}\sin(\chi), \quad J_G = \frac{\pi\Delta_0^2\mathcal{A}_B}{4e\rho_S T_C\xi_S(T)}, \tag{23}$$

$$\frac{J_S(0)}{J_G} = \frac{J_S(d_F)}{J_G} = \frac{\Gamma(p-q)}{2\Delta_0^2}\delta_s(0)\delta_S(d_F)\sin(\varphi - \chi), \tag{24}$$

where $\Delta_0 = \sqrt{8\pi^2 T_C(T_C - T)/7\zeta(3)}$ is the bulk value of the order parameter in the S electrodes, $\mathcal{A}_B$ is the cross-sectional area of the structure, and $\zeta(z)$ is the Riemann zeta function. Here

$$\delta_s(0) = \frac{2b(p-q)\cos(\varphi-\chi) - 2a(p+q)}{\Gamma[(p+q)^2 - (p-q)^2\cos^2(\varphi-\chi)]}, \tag{25}$$

$$\delta_S(d_F) = \frac{2b(p+q) - 2a(p-q)\cos(\varphi-\chi)}{\Gamma[(p+q)^2 - (p-q)^2\cos^2(\varphi-\chi)]} \tag{26}$$

are the order parameters at the sF and FS interfaces, respectively [see Fig. 1(b)], and

$$a = -\delta_s(-d_s)\sqrt{1 - \frac{\delta_s^2(-d_s)}{2\Delta_0^2}}, \quad b = \frac{\Delta_0}{\sqrt{2}}, \tag{27}$$

where $\delta_s(-d_s)$ is the solution of the transcendental equation

$$K\left(\frac{\delta_s(-d_s)}{\Delta_0\eta}\right) = \frac{d_s\eta}{\sqrt{2}\xi_s(T)}, \quad \eta = \sqrt{2 - \frac{\delta_s^2(-d_s)}{\Delta_0^2}}. \tag{28}$$

Here, $K(z)$ is the complete elliptic integral of the first kind. Substitution of $\delta_s(-d_s) = 0$ into Eq. (28) leads to the expression for the critical s layer thickness $d_{sc} = (\pi/2)\xi_S(T)$, which was used above.

For the calculation of the CPR we need to exclude the phase χ of the intermediate s layer from the expressions for the currents (23) and (24). The value of this phase is determined from the condition that the currents flowing across the Is and sF interfaces should be equal to each other.

For large thickness of the middle s electrode ($d_s \gg d_{sc}$) the magnitude of the order parameter $\delta_s(-d_s)$ is close to that of the bulk material Δ_0 and we may put $a = -b$ in Eqs. (25) and (26),

$$\delta_S(d_F) = \delta_s(0) = \frac{\sqrt{2}\Delta_0}{\Gamma[(p+q) - (p-q)\cos(\varphi-\chi)]}, \tag{29}$$

resulting in

$$J_S(0) = J_S(d_F) = \frac{J_G \beta \sin(\varphi - \chi)}{\Gamma[1 - \beta\cos(\varphi - \chi)]} \tag{30}$$

together with the equation to determine χ

$$\frac{\Gamma}{\Gamma_{BI}} \sin(\chi) = \frac{\beta \sin(\varphi - \chi)}{1 - \beta\cos(\varphi - \chi)}, \quad \beta = \frac{p - q}{p + q}. \tag{31}$$

From (29), (30), and (31) it follows that in this mode the SIsFS structure can be considered as a pair of SIs and sFS junctions connected in series. Therefore, the properties of the structure are almost independent of the thickness d_s and are determined by the junction with the smallest critical current.

Indeed, we can conclude from (31) that the phase χ of the s layer order parameter depends on the ratio of the critical current, $I_{CSIs} \propto \Gamma_{BI}^{-1}$, of its SIs part to that, $I_{CsFS} \propto |\beta|\Gamma^{-1}$, of the sFS junction. The coefficient β in (31) is a function of the F layer thickness, which becomes close to unity in the limit of small d_F and exhibits damped oscillations with increase in d_F [see the analytical expression for β (21)]. That means that there is a range of thicknesses d_{Fn}, determined by the equation $\beta = 0$, at which $J_S \equiv 0$, and there is a transition from the 0 to the π state in the sFS part of the SIsFS junction. In other words, crossing the value d_{Fn} with an increase of d_F provides a π shift of χ relative to the phase of the S electrode.

In Fig. 2 we clarify the classification of the operation modes and demonstrate the phase diagram in the (d_s, d_F) plane, which follows from our analytical results (21)–(28). The calculations have been done at $T = 0.9T_C$ for $h = H/\pi T_C = 10$, $\Gamma_{BI} = 200$, and $\Gamma = 5$. The structures with s layer smaller than the critical thickness $d_{sc} = \pi\xi_S(T)/2$ correspond to the mode 2 with fully suppressed superconductivity in the s layer. Conversely, the top part of the diagram corresponds to the s layer in the superconductive state (mode 1). This area is divided into two parts depending on whether the weak place is located at the tunnel barrier I (mode 1a) or at the ferromagnetic F layer (mode 1b). The separating black solid vertical lines in the upper part of Fig. 2 represent the locus of points where the critical currents of the SIs and sFS parts of the SIsFS junction are equal. The dashed lines give the locations of the points of 0 to π transitions, $d_{Fn} = \pi(n - 3/4)\xi_F\sqrt{2/h}, n = 1,2,3,\ldots$, at which J_C changes its sign. In the vicinity of these points there are the valleys of mode 1b with the width $\Delta d_{Fn} \approx \xi_F \Gamma \Gamma_{BI}^{-1} h^{-1/2} \exp\{\pi(n - 3/4)\}$, embedded into the areas occupied by mode 1a. For the set of parameters used for calculation of the phase diagram presented in Fig. 2, there is only one valley with the width $\Delta d_{F1} \approx \xi_F \Gamma \Gamma_{BI}^{-1} h^{-1/2} \exp\{\pi/4\}$ located around the point $d_{F1} = (\pi/4)\xi_F\sqrt{2/h}$ of the first 0 to π transition.

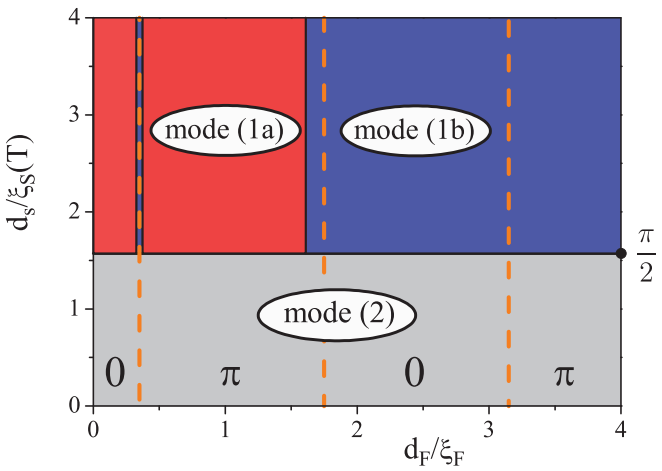

FIG. 2. (Color online) The phase diagram of the operation modes of the SIsFS structure in the (d_s, d_F) plane. The bottom area corresponds to the mode 2 with fully suppressed superconductivity in the s layer. The top part of the diagram, separated from the bottom one by the solid horizontal line, corresponds to the s layer in the superconductive state. It provides the value of the s layer critical thickness d_{sc}. The upper left part indicates the mode 1a with the weak place located at the SIs tunnel barrier. The upper right area as well as the thin valley around the first 0-π transition correspond to the mode 1b with the weak place located at the sFS junction. The solid vertical lines provide the loci of the borders between the modes 1a and 1b. The vertical dashed lines show the positions of 0-π transitions. The calculations have been done for $H = 10\pi T_C$, $\Gamma_{BI} = 200$, and $\Gamma = 5$ at $T = 0.9T_C$.

1. *Mode 1a: Switchable* 0-π *SIs junction*

In the experimentally realized case[8–11] $\Gamma_{BI}^{-1} \ll |\beta|\Gamma^{-1}$ the condition is fulfilled and the weak place in the SIsFS structure is located at the SIs interface. In this approximation it follows from (31) that

$$\chi \approx \varphi - \frac{2q\Gamma}{(p - q)\Gamma_{BI}} \sin(\varphi)$$

in the 0 state ($d_F < d_{F1}$) and

$$\chi \approx \pi + \varphi - \frac{2q\Gamma}{(p - q)\Gamma_{BI}} \sin(\varphi)$$

in the π state ($d_F > d_{F1}$). Substitution of these expressions into (30) results in

$$J_S(\varphi) = \pm\frac{J_G}{\Gamma_{BI}}\left[\sin\varphi - \frac{\Gamma}{\Gamma_{BI}}\frac{1 \mp \beta}{2\beta}\sin(2\varphi)\right] \tag{32}$$

for the 0 and π states, respectively. It is seen that for $d_F < d_{F1}$ the CPR (32) has the sinusoidal shape typical for SIS tunnel junctions with a small correction taking into account the suppression of superconductivity in the s layer due to proximity with the FS part of the complex sFS electrode. Its negative sign is typical for tunnel Josephson structures with composite NS or FS electrodes.[39,40] For $d_F > d_{F1}$ the supercurrent changes its sign, thus exhibiting the transition of the SIsFS junction into the π state. It is important to note that in this mode the SIsFS structure may have almost the same value of the critical current in both 0 and π states. For this reason we have identified this mode as a "switchable 0-π SIS junction."

2. *Mode 1b: sFS junction*

Another limiting case is realized under the condition $\Gamma_{BI}^{-1} \gg |\beta|\Gamma^{-1}$. It is satisfied in the vicinity of the points of 0 to π transitions, d_{Fn}, and for large d_F values and high exchange fields H. In this mode (see Fig. 2) the weak place shifts to the sFS part of the SIsFS device and the structure transforms into a conventional SFS junction with a complex SIs electrode.

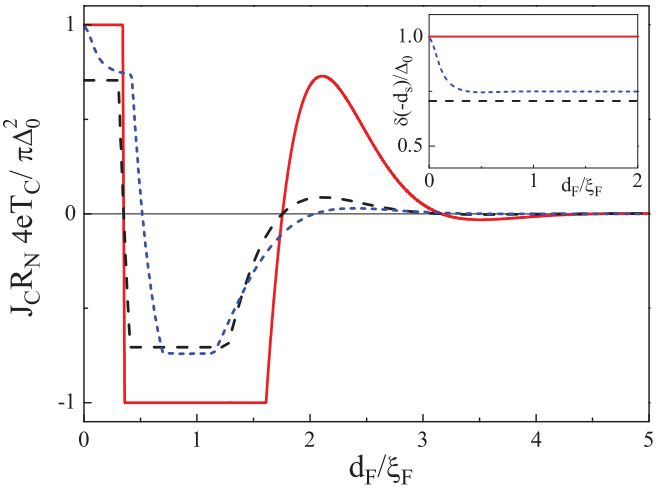

FIG. 3. (Color online) Critical current J_C of the SIsFS structure versus F layer thickness d_F calculated at $T = 0.9T_C$, $H = 10\pi T_C$, $\Gamma_{BI} = 200$, and $\Gamma = 5$ for s layer thickness $d_s = 2\xi_S(T)$ slightly above the critical one d_{sc}. The inset shows the dependence of the pair potential $\delta_s(-d_s)$ at the Is interface of the s layer versus the F layer thickness d_F. The solid lines have been calculated for $d_s \gg d_{sc}$ from Eqs. (32) and (33). The dashed line is the result of calculations using the analytical expressions (23)–(28) for the thickness of the s layer $d_s = 2\xi_S(T)$. The short-dashed line is the result of numerical calculations in the frame of the Usadel equations (2)–(11).

In the first approximation on $\Gamma/(\beta\Gamma_{BI}) \gg 1$ it follows from (30) and (31) that

$$\chi = \frac{\Gamma_{BI}}{\Gamma}\frac{\beta\sin(\varphi)}{1-\beta\cos(\varphi)},$$

resulting in

$$J_S(\varphi) = \frac{J_G\beta}{\Gamma(1-\beta\cos\varphi)}\left(\sin\varphi - \frac{\Gamma_{BI}}{2\Gamma}\frac{\beta\sin(2\varphi)}{(1-\beta\cos\varphi)}\right). \tag{33}$$

The shape of the CPR for $\chi \to 0$ coincides with that previously found in SNS and SFS Josephson devices.[37] It transforms to the sinusoidal form for sufficiently large thickness of the F layer. For small thickness of the F layer as well as in the vicinity of 0-π transitions, significant deviations from the sinusoidal form may occur.

The transition between modes 1a and the 1b is also demonstrated in Fig. 3. It shows the dependence of the critical current J_C across the SIsFS structure versus the F layer thickness d_F. The inset in Fig. 3 demonstrates the magnitude of the order parameter at the Is interface as a function of d_F. The solid lines in Fig. 3 give the shape of $J_C(d_F)$ and $\delta_0(-d_s)$ calculated from (32) and (33). These equations are valid in the limit $d_s \gg d_{sc}$ and do not take into account possible suppression of superconductivity in the vicinity of a tunnel barrier due to proximity with the FS part of the device. The dashed lines are the result of calculations using the analytical expressions (23)–(28) for the thickness of the s layer $d_s = 2\xi_S(T)$, which slightly exceeds the critical one, $d_{sc} = (\pi/2)\xi_S(T)$. These analytical dependencies are calculated at $T = 0.9T_C$ for $H = 10\pi T_C$, $\Gamma_{BI} = 200$, $\Gamma = 5$, and $\gamma_B = 0$. The short-dashed curves are the results of numerical calculations performed self-consistently in the frame of the Usadel equations (2)–(11) for the corresponding set of the parameters $T = 0.9T_C$ for $H = 10\pi T_C$, $\gamma_{BI} = 1000$, $\gamma = 1$, $\gamma_B = 0.3$, and the same thickness of the s layer $d_{sc} = (2)\xi_S(T)$. The interface parameters $\gamma_{BI} = 1000$ and $\gamma = 1$ are chosen the same as for the analytical case. The choice of $\gamma_B = 0.3$ allows one to take into account the influence of mismatch which generally occurs at the sF and FS boundaries.

It can be seen that there is a qualitative agreement between the shapes of the three curves. For small d_F the structure is in the 0-state mode-1a regime. The difference between dashed and short-dashed lines in this area is due to the fact that the inequalities (18) are not fulfilled for very small d_F. The solid and short-dashed curves start from the same value since for $d_F = 0$ the sFS electrode becomes a single spatially homogeneous superconductor. For $d_s = 2\xi_S(T)$ the intrinsic superconductivity in the s layer is weak and is partially suppressed with d_F increase (see the inset in Fig. 3). This suppression is accompanied by a rapid drop of the critical current. It can be seen that starting from the value $d_F \approx 0.4\xi_F$ our analytical formulas (23)–(28) are accurate enough. The larger is d_s, the better is the agreement between numerical and analytical results due to the better applicability of the GL equations in the s layer. With further d_F increase the structure passes through a valley of the mode-1b state, located in the vicinity of the 0-to-π transition, and comes into the π state of mode 1a. Finally for $d_F \gtrsim 1.6\xi_F$ there is a transition from mode 1a to mode 1b, which is accompanied by damped oscillations of $J_C(d_F)$ with increase in d_F.

B. Mode 2: SInFS junction $d_s \leqslant d_{sc}$

For $d_s \leqslant d_{sc}$ intrinsic superconductivity in the s layer is completely suppressed, resulting in formation of the complex InF weak-link area, where n marks the intermediate s film in the normal state. In this parameter range the weak link is always located in the tunnel barrier and the CPR has sinusoidal shape,

$$J_S(\varphi) = \frac{J_G}{\sqrt{2}}\frac{(p-q)\sin\varphi}{2pq\Gamma\Gamma_{BI}\cos\frac{d_s}{\xi_s(T)} + [2pq\Gamma + (p+q)\Gamma_{BI}]\sin\frac{d_s}{\xi_s(T)}}. \tag{34}$$

In the vicinity of the critical thickness $d_s \lesssim d_{sc}$, the factor $\cos[d_s/\xi_S(T)]$ in (34) is small and the supercurrent is given by the expression

$$J_S(\varphi) = \frac{J_G}{2\sqrt{2}}\frac{(p-q)\sin\varphi}{2pq\Gamma + (p+q)\Gamma_{BI}}. \tag{35}$$

Further decrease of d_s to the limit $d_s \ll d_{sc}$ leads to

$$J_S(\varphi) = \frac{J_G}{\sqrt{2}}\frac{(p-q)\sin\varphi}{2pq\Gamma\Gamma_{BI}}. \tag{36}$$

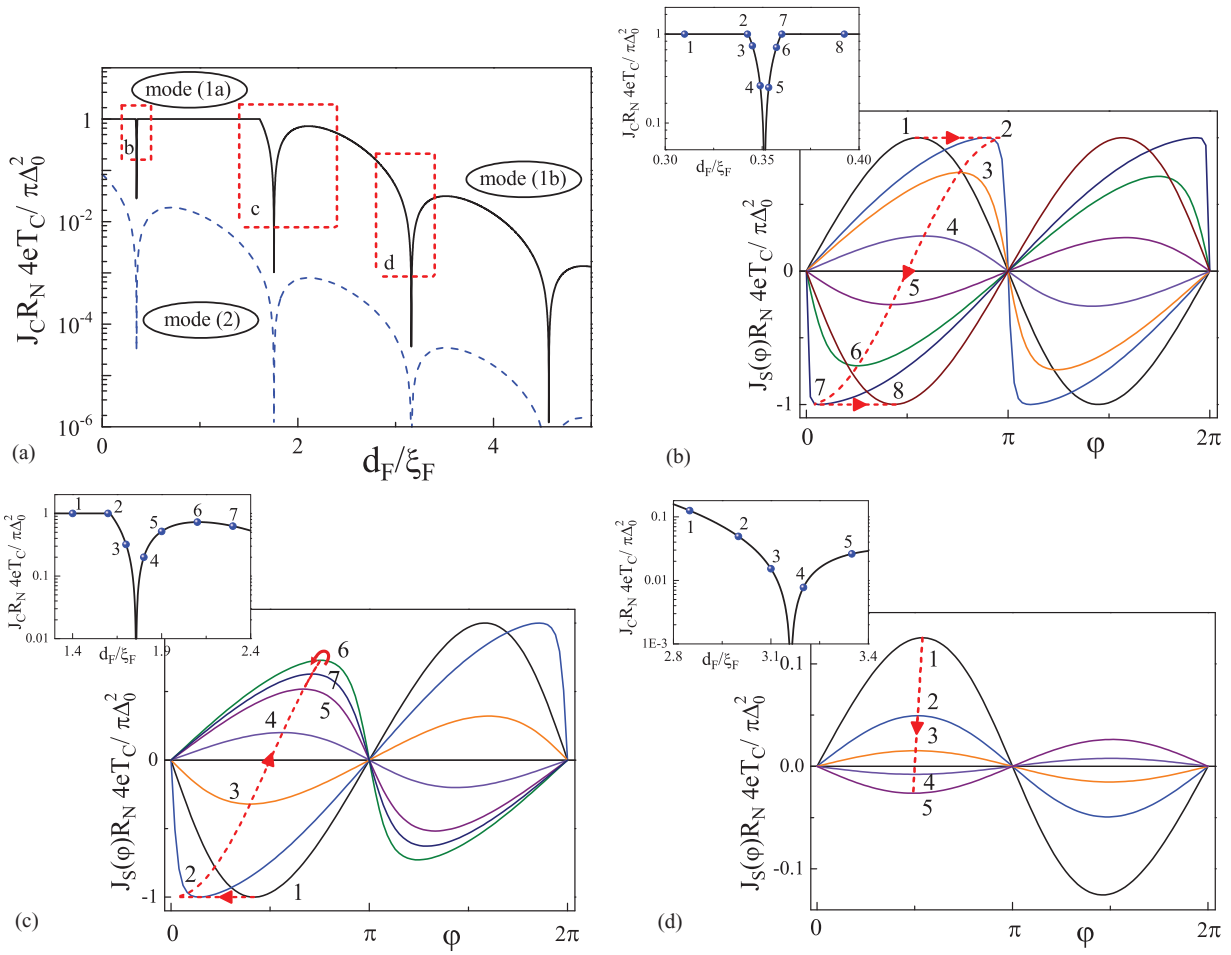

FIG. 4. (Color online) (a) Magnitude of the critical current J_C in the SIsFS structure versus F layer thickness d_F for two thickness of the middle s layer, $d_s = 5\xi_S(T) > d_{sc}$ (solid line) and $d_s = 0.5\xi_S(T) < d_{sc}$ (dashed line) calculated at $T = 0.9T_C$ for $H = 10\pi T_C$, $\Gamma_{BI} = 200$, and $\Gamma = 5$. (b)–(d) CPRs in the vicinity of 0-π transitions. The corresponding insets show the enlarged parts of the $J_C(d_F)$ dependence enclosed in rectangles (a) and marked by the letters b–d, respectively. The digits on the insets show the points at which the $J_S(\varphi)$ curves have been calculated. The dashed lines in (b)–(d) are the loci of critical points at which the $J_S(\varphi)$ dependence reaches its maximum value $J_C(d_F)$.

The magnitude of the critical current in (36) is close to that in the well-known case of SIFS junctions in the appropriate regime.

C. Current-phase relation

In the previous section we have demonstrated that variation in the thickness of the ferromagnetic layer should lead to the transformation of the CPR of the SIsFS structure. Figure 4(a) illustrates the $J_C(d_F)$ dependencies calculated from expressions (23)–(28) at $T = 0.9T_C$ for $H = 10\pi T_C$, $\gamma_B = 0$, $\Gamma_{BI} \approx 200$, and $\Gamma \approx 5$ for two thickness of the s layer $d_s = 5\xi_S(T)$ (solid line) and $d_s = 0.5\xi_S(T)$ (dashed line). In Figs. 4(b)–4(d) we enlarge the parts of the $J_C(d_F)$ dependence enclosed in rectangles labeled by the letters b, c, and d in Fig. 4(a) and mark by digits the points where the $J_S(\varphi)$ curves have been calculated. These curves are marked by the same digits as the points in the enlarged parts of the $J_C(d_F)$ dependencies. The dashed lines in Figs. 4(b)–4(d) are the loci of critical points at which the $J_S(\varphi)$ dependence reaches its maximum value $J_C(d_F)$.

Figure 4(b) presents the mode-1b valley, which divides the mode-1a domain into 0- and π- state regions. In the mode-1a domain the SIsFS structure behaves as SIs and sFS junctions connected in series. Its critical current equals the minimal one among the critical currents of the SIs (J_{CSIs}) and sFS (J_{CsFS}) parts of the device. In the considered case the thickness of the s film is sufficiently large to prevent suppression of superconductivity. Therefore, J_{CSIs} does not change when moving from point 1 to point 2 along the $J_C d_F$ dependence curve. At point 2, when $J_{CSIs} = J_{CsFS}$, we arrive at the border between modes 1a and 1b. It is seen that at this point there is maximum deviation of $J_S(\varphi)$ from the sinusoidal shape. Further increase of d_F leads to the 0-π transition, when the parameter β in (33) becomes small and $J_S(\varphi)$ is almost restored to its sinusoidal shape. Beyond the area of the 0-to-π transition, the critical current changes its sign and the CPR starts to deform again. The deformation achieves its maximum at the point 7 located at the other border between modes 1a

and 1b. The displacement from point 7 to point 8 along the $J_C(d_F)$ dependence leads to recovery of a sinusoidal CPR.

Figure 4(c) presents the transition from the π state of mode 1a to mode 1b with d_F increase. It is seen that the offset from point 1 to points 2–5 along $J_C(d_F)$ results in a transformation of the CPR similar to that shown in Fig. 4(b) during displacement in the direction from point 1 to points 2–6. The only difference is the starting negative sign of the critical current. However, this behavior of the CPR along with the close transition between modes lead to formation of a well-pronounced kink in the $J_C(d_F)$ dependence. Furthermore, in contrast to Fig. 4(b) at point 6, the junction is still in mode 1b and remains in this mode with further increase in d_F. At point 6 the critical current achieves its maximum value and it decreases along the dashed line for larger d_F.

Figure 4(d) shows the transformation of the CPR in the vicinity of the next 0-to-π transition in mode 1b. There is a small deviation from the sinusoidal shape at point 1, which vanishes exponentially with an increase of d_F.

In mode 2 [the dashed curve in Fig. 4(a)] intrinsic superconductivity in the s layer is completely suppressed, resulting in the formation of a complex InF weak-link region, and the CPR becomes sinusoidal (34).

IV. ARBITRARY TEMPERATURE

At arbitrary temperatures the boundary problem (2)–(11) goes beyond the assumptions of GL formalism and requires a self-consistent solution. We have performed it numerically in terms of the nonlinear Usadel equations in an iterative manner. All calculations were performed for $T = 0.5T_C$, $\xi_S = \xi_F$, $\gamma_{BI} = 1000$, $\gamma_{BFS} = 0.3$, and $\gamma = 1$.

Calculations show that at the selected transparency of the tunnel barrier ($\gamma_{BI} = 1000$) the suppression of superconductivity in the left electrode is negligibly small. This allows one to select the thickness of the left S electrode $d_{SL} = 2\xi_S$ without any loss of generality. On the contrary, proximity of the right S electrode to the F layer results in strong suppression of superconductivity at the FS interface. Therefore the pair potential of the right S electrode reaches its bulk value only at thickness $d_{SR} \gtrsim 10\xi_S$. It is for these reasons we have chosen $d_{SR} = 10\xi_S$ for the calculations.

Furthermore, the presence of a low-transparency tunnel barrier in the considered SIsFS structures limits the magnitude of the critical current J_C by a value much smaller than the depairing current of the superconducting electrodes. This allows one to neglect nonlinear corrections to coordinate dependence of the phase in the S banks.

The results of the calculations are summarized in Fig. 5. Figure 5(a) shows the dependence of J_C of the SIsFS structure on the F layer thickness d_F for relatively large $d_s = 5\xi_S$ (solid) and small $d_s = 0.5\xi_S$ (dashed) s film thickness. The letters on the curves indicate the points at which the coordinate dependencies of the magnitude of the order parameter, $|\Delta(x)|$, and phase difference across the structure, χ, have been calculated for the phase difference $\varphi = \pi/2$. These curves are shown in Figs. 5(b)–5(f) as the upper and lower plots, respectively. There is direct correspondence between the letters, b, c, d, e, and f on the $J_C(d_F)$ curves and the labels (b), (c), (d), (e), and (f) of the panels.

It is seen that the qualitative behavior of the $J_C(d_F)$ dependence at $T = 0.5T_C$ remains similar to that obtained in the frame of the GL equations for $T = 0.9T_C$ [see Fig. 4(a)]. Furthermore, the modes of operation discussed above remain relevant too. Figures 5(b)–5(f) make this statement more clear.

At the point marked by the letter b, the s film is sufficiently thick, $d_s = 5\xi_S$, while the F film is rather thin, $d_F = 0.3\xi_F$, and therefore the structure is in the 0 state of mode 1a. In this regime the phase mainly drops across the tunnel barrier, while the phase shifts at the s film and in the S electrodes are negligibly small [see the bottom plot in Fig. 5(b)].

At the point marked by the letter c ($d_s = 5\xi_S$, $d_F = \xi_F$), the structure is in the π state of mode 1a. It is seen from Fig. 5(c) that there is a phase jump at the tunnel barrier and an additional π shift occurs between the phases of the S and s layers.

For $d_F = 3\xi_F$ [Fig. 5(d)] the position of the weak place shifts from the SIs to the sFS part of the SIsFS junction. Then the structure starts to operate in mode 1b. It is seen that the phase drop across the SIs part is small, while it is $\varphi - \chi \approx \pi/2$ across the F layer, as it should be in SFS junctions with SIs and S electrodes.

At the points marked by the letters e and f, the thickness of the s layer, $d_s = 0.5\xi_S$, is less than its critical value. Then superconductivity in the s spacer is suppressed due to the proximity with the F film and SIsFS device operates in the mode 2. At $d_F = \xi_F$ [the point e in Fig. 5(a) and the panel Fig. 5(e)] the position of the weak place is located in the SIs part of the structure and there is an additional π shift of phase across the F film. As a result, the SIsFS structure behaves like an SInFS tunnel π junction. The unsuppressed residual value of the pair potential is due to the proximity with the right S electrode and it disappears with the growth of the F layer thickness, which weakens this proximity effect. At $d_F = 3\xi_F$ [Fig. 5(f)] the weak place is located in the F part of IsF trilayer. Despite strong suppression of the pair potential in the s-layer, the distribution of the phase inside the IsF weak place has a rather complex structure, which depends on the thicknesses of the s and F layers.

A. Temperature crossover from 0 to π states

The temperature-induced crossover from 0 to π states in SFS junctions was described in Ref. 26 in structures with sinusoidal CPR. It was found that the transition takes place in a relatively broad temperature range.

Our analysis of SIsFS structure [see Fig. 6(a)] shows that the smoothness of the 0-to-π transition strongly depends on the CPR shape. Note that almost all previous theoretical results were obtained within a linear approximation, leading to a sinusoidal CPR. To prove the dependence on the CPR shape, we have calculated numerically the set of $J_C(T)$ curves for a number of F layer film thicknesses d_F. We have chosen the thickness of the intermediate superconductor $d_s = 5\xi_S$ in order to have the SIsFS device in mode 1a and we have examined the parameter range $0.3\xi_F \leqslant d_F \leqslant \xi_F$, in which the structure exhibits the first 0-to-π transition. The borders of the d_F range are chosen in such a way that the SIsFS contact is in either the 0 ($d_F = 0.3\xi_F$) or the π ($d_F = \xi_F$) state in the whole temperature range. The corresponding $J_C(T)$ dependencies [dashed lines in Fig. 6(a)] provide the envelope of a set of

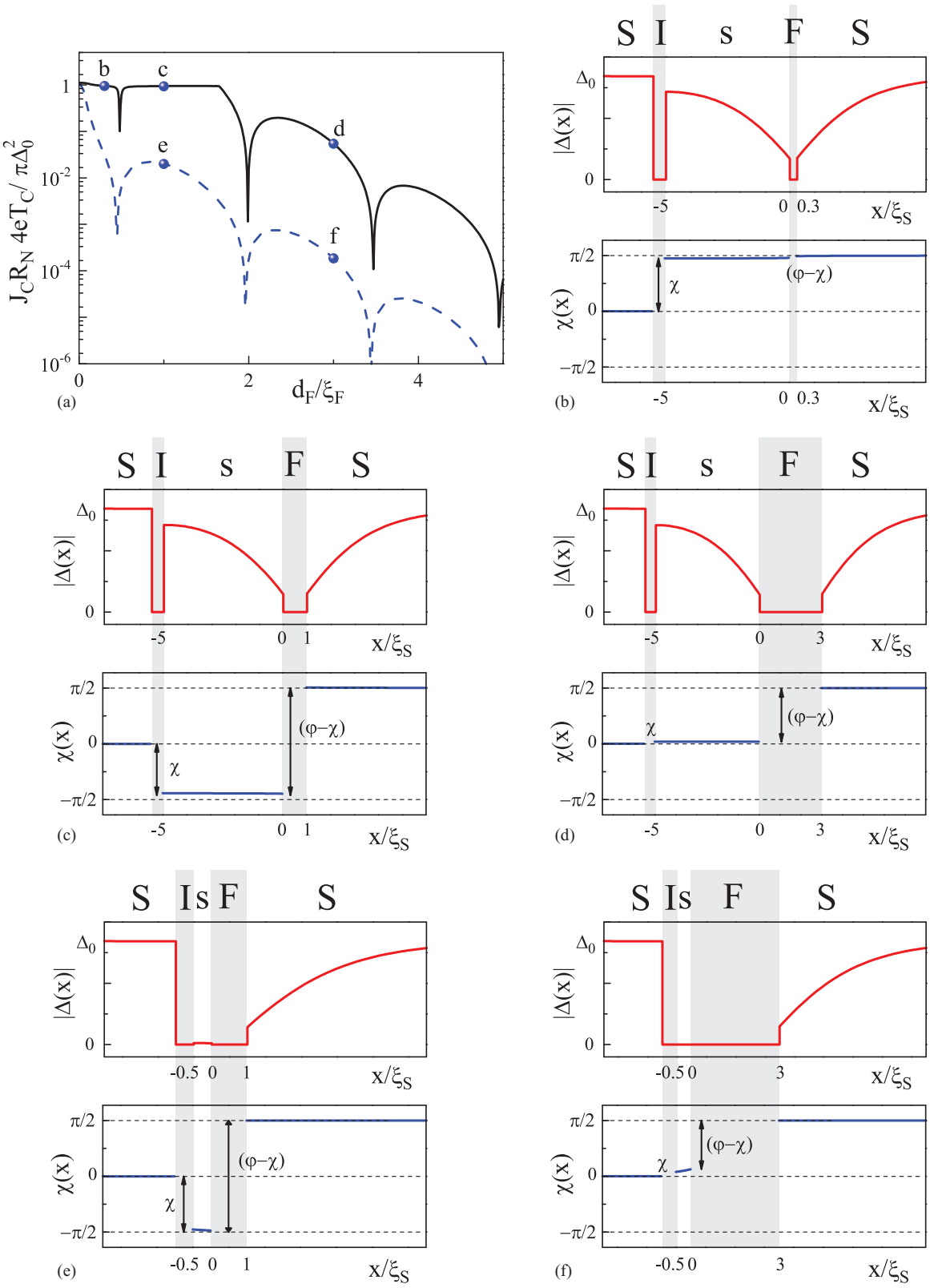

FIG. 5. (Color online) (a) Magnitude of critical current J_C of the SIsFS structure versus F layer thickness d_F calculated at $T = 0.5T_C$ for $H = 10\pi T_C$, $\gamma_{BI} = 1000$, $\gamma = 1$, and two thicknesses of the s film $d_s = 5\xi_S$ (solid line) and $d_s = 0.5\xi_S$ (dashed line). The letters on $J_C(d_F)$ give the points at which the coordinate dependencies of the magnitude of the order parameter, $|\Delta(x)|$, and phase difference across the structure, χ, have been calculated. These curves are shown in the panels (b)–(f) as the upper and lower panels, respectively.

$J_C(T)$ curves calculated for the considered range of d_F. It is clearly seen that in the vicinity of T_C the decrease of d_F results in creation of the temperature range where the 0 state exists. The point of 0-to-π transition shifts to lower temperatures

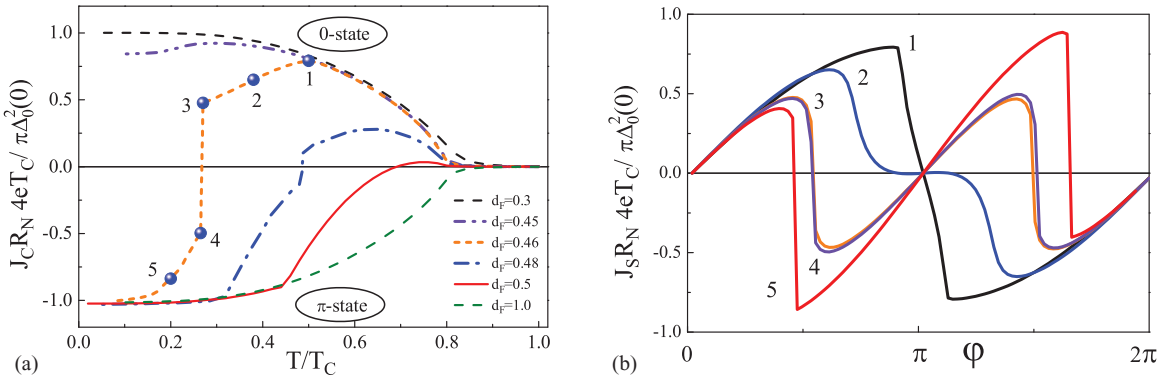

FIG. 6. (Color online) (a) Critical current J_C of the SIsFS structure versus temperature T for various F layer thicknesses d_F in the vicinity of the 0 to π transition. The dashed envelopes show the temperature dependence in the 0 (top) and π (bottom) states. (b) CPR of the structure with $d_F = 0.46\xi_F$ for a set of temperatures in the vicinity of the 0-π transition. Each curve corresponds to the point marked in (a). Note that the curves 3 and 4 almost coincide but correspond to different ground states of the junction, 0 and π, respectively. The calculations have been performed numerically for $d_s = 5\xi_S$, $H = 10\pi T_C$, $\gamma_{BI} = 1000$, $\gamma_B = 0.3$, and $\gamma = 1$.

with decreasing d_F. For $d_F \gtrsim 0.5\xi_F$ the transition is rather smooth since for $T \geqslant 0.8T_C$ the junction stays in mode 2 (with suppressed superconductivity) and deviations of the CPR from $\sin(\varphi)$ are small. Thus the behavior of the $J_C(T)$ dependencies in this case can be easily described by the analytical results from Sec. III C.

The situation drastically changes at $d_F = 0.46\xi_F$ [short-dashed line in Fig. 6(a)]. For this thickness the point of the 0-to-π transition shifts to $T \approx 0.25T_C$. This shift is accompanied by an increase of the amplitudes of the higher harmonics of the CPR [see Fig. 6(b)]. As a result, the shape of the CPR is strongly modified, so that in the interval $0 \leqslant \varphi \leqslant \pi$ the CPR curves are characterized by two values J_{C1} and J_{C2}, as is known from the case of SFcFS junctions, where "c" is a constriction.[41] In general, J_{C1} and J_{C2} differ both in sign and in magnitude and $J_C = \max(|J_{C1}|, |J_{C2}|)$. For $T > 0.25T_C$ the junction is in the 0 state and J_C grows with decrease of T up to $T \approx 0.5T_C$. Further decrease of T is accompanied by suppression of the critical current. In the vicinity of $T \approx 0.25T_C$ the difference between $|J_{C1}|$ and $|J_{C2}|$ becomes negligible and the system starts to develop an instability that eventually shows up as a sharp jump from the 0 to the π state. After the jump, $|J_C|$ continuously increases as T goes to zero.

It is important to note that this behavior should always be observed in the vicinity of a 0-π transition, i.e., in the range of parameters in which the amplitude of the first harmonic is small compared to higher harmonics. However, the closer the temperature is to T_C, the less pronounced are the higher CPR harmonics and the smaller is the magnitude of the jump. This fact is illustrated by the dash-dotted line showing $J_C(T)$ calculated for $d_F = 0.48\xi_F$. A jump in the curves calculated for $d_F \geqslant 0.5\xi_F$ also exists, but it is small and cannot be resolved on the scale used in Fig. 6(a).

At $d_F = 0.45\xi_F$ (dash-dot-dotted line in Fig. 6) the junction is always in the 0 state and there is only small suppression of the current at low temperatures despite the realization of a nonsinusoidal CPR. Thus the calculations clearly show that it is possible to realize a set of parameters of SIsFS junctions where thermally induced 0-π crossover can be observed and controlled by temperature variation.

B. 0-to-π crossover by changing the effective exchange energy in an external magnetic field

The exchange field is an intrinsic microscopic parameter of a ferromagnetic material which cannot be controlled directly by application of an external field. However, spin splitting in F layers can be provided by both an internal exchange field and an external magnetic field,[42,43] resulting in generation of an effective exchange field, which is equal to their sum. The practical realization of this effect is a challenge since it is difficult to fulfill the special requirements[42,43] on the thickness of the S electrodes and the SFS junction geometry.

Another opportunity can be realized in soft diluted ferromagnetic alloys like $Fe_{0.01}Pd_{0.99}$. Investigations of the magnetic properties[44] of these materials have shown that below 14 K they exhibit ferromagnetic order due to the formation of weakly coupled ferromagnetic nanoclusters. In the clusters, the effective spin polarization of the Fe ions is about $4\mu_B$, corresponding to that in the bulk Pd_3Fe alloy. It was demonstrated that the hysteresis loops of $Fe_{0.01}Pd_{0.99}$ films have the form typical of nanostructured ferromagnets with weakly coupled grains (the absence of domains; a small coercive force; a small interval of magnetization reversal, where the magnetization changes its direction following changes in the applied magnetic field; and a prolonged part, where the component of the magnetization vector along the applied field grows gradually).

The small concentration of the Pd_3Fe clusters and their ability to follow variations in the applied magnetic field may result in generation of $H_{\rm eff}$, which is of the order of

$$H_{\rm eff} \approx H\frac{n_\uparrow V_\uparrow - n_\downarrow V_\downarrow}{nV}. \qquad (37)$$

Here n is the average concentration of electrons within a physically small volume V, in which one performs an averaging of the Green's functions in the transformation to a quasiclassical description of superconductivity, and $n_{\uparrow,\downarrow}$ and $V_{\uparrow,\downarrow}$ are the values describing the spin-polarized parts of n and of the volume V, which they occupy, respectively. A similar kind of $H_{\rm eff}$ nucleates in NF or SF proximity structures, which are composed from thin layers.[45–48] There is an interval of

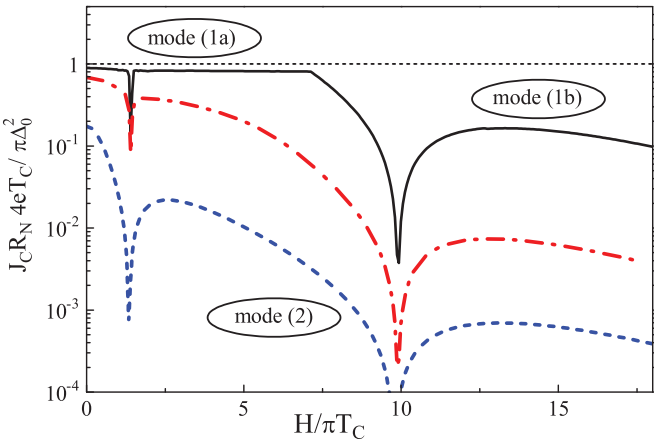

FIG. 7. (Color online) The magnitude of critical current J_C of the SIsFS structure versus exchange field H for thick $d_s = 5\xi_S$ (solid), thin $d_s = 0.5\xi_S$ (dashed) and intermediate $d_s = 3\xi_S$ (dash-dotted) s-layer thickness. The plot demonstrates the possibility of 0-π transition by varying the effective exchange field. The calculations have been performed for $T = 0.5T_C$, $d_F = 2\xi_F$, $\gamma_{BI} = 1000$, $\gamma_B = 0.3$, $\gamma = 1$.

applied magnetic fields $H_{\rm ext}$ where the alloy magnetization changes its direction and the concentrations $n_{\uparrow,\downarrow}$ depend on the prehistory of application of the field,[10,12] providing the possibility to control $H_{\rm eff}$ by an external magnetic field.

Derivation of the possible relationships between $H_{\rm eff}$ and $H_{\rm ext}$ is outside the scope of this paper. Below we will concentrate only on an assessment of the intervals in which $H_{\rm eff}$ should be changed to ensure the transition of a SIsFS device from the 0 to the π state. To do this, we calculate the $J_C(H)$ dependencies presented in Fig. 7. The calculations have been done for a set of structures with $d_F = 2\xi_F$ and s film thickness ranging from thick, $d_s = 5\xi_S$ (solid line), to an intermediate value $d_s = 2\xi_S$ (dash-dotted line) and finishing with a thin film having $d_s = 0.5\xi_S$ (dashed line). It is clearly seen that these curves have the same shape as the $J_C(d_F)$ dependencies presented in Sec. III. For $d_s = 5\xi_S$ and $H \lesssim 7\pi T_C$ the magnitude of J_C is almost independent of H, but it changes sign at $H \approx 1.25\pi T_C$ due to the 0-π transition. It is seen that for the transition, while maintaining the normalized current value at a level close to unity, changes of H are required approximately of the order of $0.1\pi T_C$ or 10%. For $d_s = 2\xi_S$ and $H \lesssim 3\pi T_C$, it is necessary to change H by 20% to realize such a transition. In this case the value of the normalized current is at the level 0.4. In mode 2 the transition requires a 100% change of H, which is not practical.

V. DISCUSSION

We have performed a theoretical study of magnetic SIsFS Josephson junctions. At $T \leqslant T_C$ calculations have been performed analytically in the frame of the GL equations. For arbitrary temperatures we have developed a numerical code for self-consistent solution of the Usadel equations. We have outlined several modes of operation of these junctions. For the s layer in the superconducting state they are S-I-sfS or SIs-F-S devices with the weak place located at the insulator (mode 1a) or at the F layer (mode 1b), respectively. For a small s layer thickness, its intrinsic superconductivity is completely suppressed, resulting in formation of an InF weak place (mode 2). We have examined the shape of $J_S(\varphi)$ and the spatial distribution of the modulus of the pair potential and its phase difference across the SIsFS structure in these modes.

For mode 1 the shape of the CPR can substantially differ from sinusoidal even in the vicinity of T_C. The deviations are largest when the structure is close to the crossover between the modes 1a and 1b. This effect results in kinks in the dependencies of J_C on temperature and on parameters of the structure (thickness of the layers d_F,d_s and exchange energy H) as illustrated in Fig. 4 on $J_C(d_F)$ curves. The transformation of the CPR is even more important at low temperatures. For $T \lesssim 0.25T_C$ a sharp 0-π transition can be realized induced by a small temperature variation (Fig. 6). This instability must be taken into account when using the structures as memory elements. On the other hand, this effect can be used in detectors of electromagnetic radiation, where absorption of a photon in the F layer will provide local heating leading to development of an instability and subsequent phonon registration.

We have shown that suppression of the order parameter in a thin s film due to the proximity effect leads to decrease of the product $J_C R_N$ in both 0 and π states. On the other hand, the proximity effect may also support s layer superconductivity due to the impact of S electrodes. In mode 1a the product $J_C R_N$ in 0 and π states can achieve values typical for SIS tunnel junctions.

In mode 2 a sinusoidal CPR is realized. Despite that, the distribution of the phase difference $\chi(x)$ in the IsF weak place may have a complex structure, which depends on the thickness of the s and F layers. These effects should influence the dynamics of a junction in its ac state and deserve further study.

Further, we have also shown that in mode 1a nearly 10% change in the exchange energy can cause a 0-π transition, i.e., changing the sign of the product $J_C R_N$, while maintaining its absolute value. This unique feature can be implemented in mode 1a, since in it changes of the exchange energy determine only the presence or absence of a π shift between s and S electrodes and do not affect the magnitude of the critical current of the SIs part of the SIsFS junction.

In mode 1b, the F layer becomes a part of the weak-link area. In this case the π shift initiated by the change in H must be accompanied by changes of the magnitude of J_C due to the oscillatory nature of superconducting correlations in the F film. The latter may lead to a very complex and irregular dependence $J_C(H_{\rm ext})$, such as has been observed in Nb-PdFe-Nb SFS junctions (see Fig. 3 in Ref. 8). In contrast, the $J_C(H_{\rm ext})$ curves of a SIsFS structure with the same PdFe metal do not demonstrate these irregularities.[10,11]

To characterize a junction's stability with respect to H variations it is convenient to introduce the parameter $\eta = (dJ_C/J_C)/(dH/H)$ which relates the relative change in the critical current to the relative change in the exchange energy. The larger the magnitude of η the more intense irregularities in a SFS junction are expected with variation of H. In Fig. 8 we compare SIsFS devices with conventional SFS, SIFS, and SIFIS junctions making use of two of the most important parameters: the instability parameter η and the product $J_C R_N$, the value of which characterizes high-frequency properties of

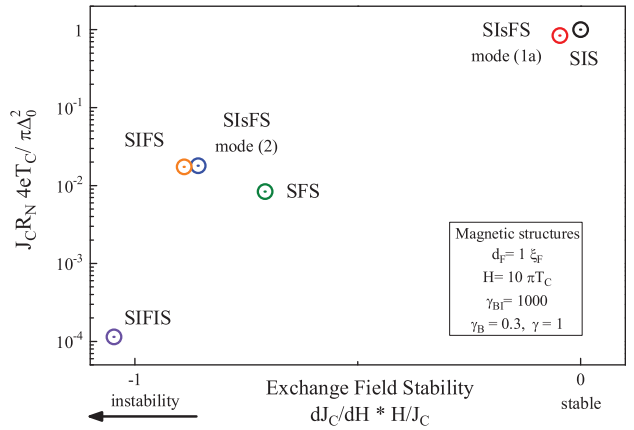

FIG. 8. (Color online) Comparison of different types of Josephson structures, marked by points on the phase plane, in terms of $J_C R_N$ and exchange field stability η. All calculations have been performed for $T = 0.5T_C$, $d_F = \xi_F$, $\gamma_{BI} = 1000$, $\gamma_B = 0.3$, and $\gamma = 1$. For SIsFS structures $d_s = 5\xi_S$ and $d_s = 0.5\xi_S$ are taken in mode 1a and mode 2, respectively.

the structures. The calculations have been done in the frame of the Usadel equations for the same set of junction parameters, namely, $T = 0.5T_C$, $H = 10\pi T_C$, $d_F = \xi_F$, $\gamma_{BI} = 1000$, $\gamma_B = 0.3$, and $\gamma = 1$.

It can be seen that the presence of two tunnel barriers in a SIFIS junction results in the smallest $J_C R_N$ and strong instability. The SIFS and SIsFS structures in mode 2 demonstrate better results with almost the same parameters. Conventional SFS structures have a twice smaller $J_C R_N$ product, having a higher critical current but lower resistivity. At the same time, SFS junctions are more stable due to the lack of a low-transparency tunnel barrier. The latter is the main source of instability due to sharp phase discontinuities at the barrier I.

In contrast to the standard SFS, SIFS, and SIFIS junctions, SIsFS structures achieve $J_C R_N$ and stability characteristics comparable to those of SIS tunnel junctions. This unique property is favorable for application of SIsFS structures in superconducting electronic circuits.

ACKNOWLEDGMENTS

We thank V. V. Ryazanov, V. V. Bol'ginov, I. V. Vernik, and O. A. Mukhanov for useful discussions. This work was supported by the Russian Foundation for Basic Research Grants No. 14-02-00089 A and No. 14-02-31002-mol_a, the Russian Ministry of Education and Science, the Dynasty Foundation, a Scholarship of the President of the Russian Federation, IARPA, and the Dutch FOM.

APPENDIX: BOUNDARY PROBLEM AT $T \lesssim T_C$

In the limit of high temperature

$$G_S = G_s = G_F = \mathrm{sgn}(\Omega) \tag{A1}$$

and the boundary problem reduces to a system of linearized equations. Their solution in the F layer ($0 \leqslant x \leqslant d_F$) has the form

$$\Phi_F = C \sinh \frac{\sqrt{\Theta}(x - d_F/2)}{\xi_F} + D \cosh \frac{\sqrt{\Theta}(x - d_F/2)}{\xi_F}, \tag{A2}$$

where $\Theta = \widetilde{\Omega}\,\mathrm{sgn}(\Omega)$. For transparent FS and sF interfaces ($\gamma_B = 0$), from the boundary conditions (6), (7), and (A2) it is easy to get that

$$\frac{\xi_s}{\gamma\sqrt{\Theta}}\frac{d}{dx}\Phi_s(0) = -\Phi_s(0)\coth\frac{d_F\sqrt{\Theta}}{\xi_F} + \frac{\Phi_S(d_F)}{\sinh\frac{d_F\sqrt{\Theta}}{\xi_F}}, \tag{A3}$$

$$\frac{\xi_S}{\gamma\sqrt{\Theta}}\frac{d}{dx}\Phi_S(d_F) = \Phi_S(d_F)\coth\frac{d_F\sqrt{\Theta}}{\xi_F} - \frac{\Phi_s(0)}{\sinh\frac{d_F\sqrt{\Theta}}{\xi_F}}. \tag{A4}$$

and thus reduce the problem to the solution of the Ginzburg-Landau equations in the s and S films:

$$\xi_S^2(T)\frac{d^2}{dx^2}\Delta_k - \Delta_k\left(\Delta_0^2 - |\Delta_k|^2\right) = 0, \tag{A5}$$

$$\Delta_0^2 = \frac{8\pi^2 T_C(T_C - T)}{7\zeta(3)},$$

$$J = \frac{J_G}{\Delta_0^2}\,\mathrm{Im}\left(\Delta_k^* \xi_S(T)\frac{d}{dx}\Delta_k\right), \quad J_G = \frac{\pi\Delta_0^2}{4e\rho_S T_C \xi_S(T)}, \tag{A6}$$

where $\xi_S(T) = \pi\xi_S/2\sqrt{1 - T/T_C}$ is the GL coherence length and k equals s or S for $-d_s \leqslant x \leqslant 0$ and $x \geqslant d_F$, respectively. At Is, sF, and FS interfaces the GL equations should be supplemented by boundary conditions in the form[37]

$$\xi_S(T)\frac{d}{dx}\Delta_k(z) = b(z)\Delta_k(z), \quad b(z) = \frac{\Sigma_1(z)}{\Sigma_2(z)}, \tag{A7}$$

$$\Sigma_1(z) = \sum_{\omega=-\infty}^{\infty}\xi_S(T)\frac{d}{dx}\frac{\Phi_k(z)}{\Omega^2}, \quad \Sigma_2(z) = \sum_{\omega=-\infty}^{\infty}\frac{\Phi_k(z)}{\Omega^2}, \tag{A8}$$

where $z = -d_s, 0, d_F$. In typical experimental situations, $\gamma_{BI} \gg 1$, $\gamma\sqrt{H} \gg 1$, and $d_F\sqrt{H} \gtrsim \xi_F$. In this case in the first approximation

$$\Phi_S(d_F) = 0, \quad \Phi_s(0) = 0, \quad \frac{d}{dx}\Phi_s(-d_s) = 0,$$

and in the vicinity of interfaces

$$\Phi_S(x) = \Delta_S(x) = B_S\frac{(x - d_F)}{\xi_S(T)}, \quad d_F \lesssim x \ll \xi_S(T), \tag{A9}$$

$$\Phi_s(x) = \Delta_s(x) = -B_s\frac{x}{\xi_s(T)}, \quad -\xi_S(T) \ll x \lesssim 0, \tag{A10}$$

$$\Phi_s(x) = \Delta_s(x) = \Delta_s(-d_s), \quad -d_s \lesssim x \ll -d_s + \xi_S(T), \tag{A11}$$

where B_S, B_s, and $\Delta_s(-d_s)$ are independent of the constants x. Substitution of the solutions (A9)–(A11) into (15), (A3), and (A4) gives

$$\Gamma_{BI}\xi_S(T)\frac{d}{dx}\Phi_s(-d_s) = \Delta_s(-d_s) - \Delta_0, \tag{A12}$$

$$\Phi_S(d_F) = \frac{B_s}{\Gamma\sqrt{\Theta}\sinh\frac{d_F\sqrt{\widetilde{\Omega}}}{\xi_F}} + \frac{B_S\cosh\frac{d_F\sqrt{\Theta}}{\xi_F}}{\Gamma\sqrt{\Theta}\sinh\frac{d_F\sqrt{\Theta}}{\xi_F}}, \tag{A13}$$

$$\Phi_s(0) = \frac{B_s \cosh\frac{d_F\sqrt{\Theta}}{\xi_F}}{\Gamma\sqrt{\widetilde{\Omega}}\sinh\frac{d_F\sqrt{\Theta}}{\xi_F}} + \frac{B_S}{\Gamma\sqrt{\Theta}\sinh\frac{d_F\sqrt{\Theta}}{\xi_F}}, \tag{A14}$$

$$\Gamma_{BI} = \frac{\gamma_{BI}\xi_S}{\xi_s(T)}, \quad \Gamma = \frac{\gamma_{BI}\xi_s(T)}{\xi_S}. \tag{A15}$$

From the definition (A7), (A8) of the coefficients $b(z)$ and expressions (A12)–(A14) it follows that

$$\Gamma_{BI}\xi_s(T)\frac{d}{dx}\Delta_s(-d_s) = -[\Delta_0 - \Delta_s(-d_s)], \tag{A16}$$

$$\xi_s(T)\frac{d}{dx}\Delta_s(0) = -\frac{q+p}{2}\Gamma\Delta_s(0) - \frac{q-p}{2}\Gamma\Delta_S(d_F), \tag{A17}$$

$$\xi_S(T)\frac{d}{dx}\Delta_S(d_F) = \frac{q+p}{2}\Gamma\Delta_S(d_F) + \frac{q-p}{2}\Gamma\Delta_s(0), \tag{A18}$$

where

$$p^{-1} = \frac{8}{\pi^2}\mathrm{Re}\sum_{\omega=0}^{\infty}\frac{1}{\Omega^2\sqrt{\widetilde{\Omega}}\coth\frac{d_F\sqrt{\widetilde{\Omega}}}{2\xi_F}}, \tag{A19}$$

$$q^{-1} = \frac{8}{\pi^2}\mathrm{Re}\sum_{\omega=0}^{\infty}\frac{1}{\Omega^2\sqrt{\widetilde{\Omega}}\tanh\frac{d_F\sqrt{\widetilde{\Omega}}}{2\xi_F}}. \tag{A20}$$

In the considered limit both suppression parameters $\Gamma_{BI} \gg 1$ and $\Gamma \gg 1$ are large and from relations (15), (A3), and (A4) in the first approximation on these parameters we get that the boundary conditions (A16)–(A18) can be simplified to

$$\xi_S(T)\frac{d}{dx}\Delta_s(-d_s) = 0, \quad \Delta_s(0) = 0, \quad \Delta_S(d_F) = 0. \tag{A21}$$

Taking into account that in this approximation the supercurrent $j = 0$ and $\Delta_S(\infty) = \Delta_0$ from (A5) and (A21) it follows that

$$\Delta_S(x) = \delta_S(x)\exp\{i\varphi\}, \quad \delta_S(x) = \Delta_0\tanh\frac{x - d_F}{\sqrt{2}\xi_S(T)}, \tag{A22}$$

while

$$\Delta_s(x) = \delta_s(x)\exp\{i\chi\}, \tag{A23}$$

where $\delta_s(x)$ is the solution of the transcendental equation

$$F\left(\frac{\delta_s(x)}{\delta_s(-d_s)}, \frac{\delta_s(-d_s)}{\Delta_0\eta}\right) = -\frac{x\eta}{\sqrt{2}\xi_s(T)}, \quad \eta = \sqrt{2 - \frac{\delta_s^2(-d_s)}{\Delta_0^2}}, \tag{A24}$$

and $\delta_s(-d_s)$ is a solution of the same equation at the SIs boundary $x = -d_s$,

$$K\left(\frac{\delta_s(-d_s)}{\Delta_0\eta}\right) = \frac{d_s\eta}{\sqrt{2}\xi_s(T)}. \tag{A25}$$

Here $F(y,z)$ and $K(z)$ are the incomplete and complete elliptic integrals of the first kind, respectively.

Substitution of (A22) and (A23) into (A16)–(A18) gives that in the next approximation on Γ_{BI}^{-1} and Γ^{-1}

$$J(-d_s) = J_G\frac{\delta_s(-d_s)}{\Gamma_{BI}\Delta_0}\sin(\chi), \tag{A26}$$

$$J(0) = J(d_F) = J_G\frac{\Gamma(p-q)}{2\Delta_0^2}\delta_s(0)\delta_S(d_F)\sin(\varphi - \chi), \tag{A27}$$

where

$$\delta_s(0) = -\frac{2b(q-p)\cos(\varphi-\chi) + 2a(q+p)}{\Gamma[(q+p)^2 - (q-p)^2\cos^2(\varphi-\chi)]}, \tag{A28}$$

$$\delta_S(d_F) = \frac{2b(q+p) + 2a(q-p)\cos(\varphi-\chi)}{\Gamma[(q+p)^2 - (q-p)^2\cos^2(\varphi-\chi)]} \tag{A29}$$

are the magnitudes of the order parameters at the FS interfaces, and

$$a = -\delta_s(-d_s)\sqrt{1 - \frac{\delta_s^2(-d_s)}{2\Delta_0^2}}, \quad b = \frac{\Delta_0}{\sqrt{2}}. \tag{A30}$$

The phase χ of the order parameters of the s layer is determined from equality of the currents (A26) and (A27).

[1] A. A. Golubov, M. Yu. Kupriyanov, and E. Il'ichev, Rev. Mod. Phys. **76**, 411 (2004).

[2] A. I. Buzdin, Rev. Mod. Phys. **77**, 935 (2005).

[3] F. S. Bergeret, A. F. Volkov, and K. B. Efetov, Rev. Mod. Phys. **77**, 1321 (2005).

[4] S. Oh, D. Youm, and M. Beasley, Appl. Phys. Lett. **71**, 2376 (1997).

[5] R. Held, J. Xu, A. Schmehl, C. W. Schneider, J. Mannhart, and M. Beasley, Appl. Phys. Lett. **89**, 163509 (2006).

[6] C. Bell, G. Burnell, C. W. Leung, E. J. Tarte, D.-J. Kang, and M. G. Blamire, Appl. Phys. Lett. **84**, 1153 (2004).

[7] E. Goldobin, H. Sickinger, M. Weides, N. Ruppelt, H. Kohlstedt, R. Kleiner, and D. Koelle, Appl. Phys. Lett. **102**, 242602 (2013).

[8] V. V. Bol'ginov, V. S. Stolyarov, D. S. Sobanin, A. L. Karpovich, and V. V. Ryazanov, Pis'ma Zh. Eksp. Teor. Fiz. **95**, 408 (2012) [JETP Lett. **95**, 366 (2012)].

[9] V. V. Ryazanov, V. V. Bol'ginov, D. S. Sobanin, I. V. Vernik, S. K. Tolpygo, A. M. Kadin, and O. A. Mukhanov, Phys. Procedia **36**, 35 (2012).

[10] T. I. Larkin, V. V. Bol'ginov, V. S. Stolyarov, V. V. Ryazanov, I. V. Vernik, S. K. Tolpygo, and O. A. Mukhanov, Appl. Phys. Lett. **100**, 222601 (2012).

[11] I. V. Vernik, V. V. Bol'ginov, S. V. Bakurskiy, A. A. Golubov, M. Yu. Kupriyanov, V. V. Ryazanov, and O. A. Mukhanov, IEEE Trans. Appl. Supercond. **23**, 1701208 (2013).

[12] S. V. Bakurskiy, N. V. Klenov, I. I. Soloviev, V. V. Bol'ginov, V. V. Ryazanov, I. I. Vernik, O. A. Mukhanov, M. Yu. Kupriyanov, and A. A. Golubov, Appl. Phys. Lett. **102**, 192603 (2013).

[13] T. Ortlepp, Ariando, O. Mielke, C. J. M. Verwijs, K. F. K. Foo, H. Rogalla, F. H. Uhlmann, and H. Hilgenkamp, Science **312**, 1495 (2006).

[14]V. Ryazanov, Usp. Fiz. Nauk **169**, 920 (1999) [Phys. Usp. **42**, 825 (1999)].
[15]A. K. Feofanov, V. A. Oboznov, V. V. Bol'ginov *et al*., Nat. Phys. **6**, 593 (2010).
[16]A. V. Ustinov and V. K. Kaplunenko, J. Appl. Phys. **94**, 5405 (2003).
[17]A. Buzdin and A. E. Koshelev, Phys. Rev. B **67**, 220504(R) (2003).
[18]A. E. Koshelev, Phys. Rev. B **86**, 214502 (2012).
[19]N. G. Pugach, E. Goldobin, R. Kleiner, and D. Koelle, Phys. Rev. B **81**, 104513 (2010).
[20]E. Goldobin, D. Koelle, R. Kleiner, and R. G. Mints, Phys. Rev. Lett. **107**, 227001 (2011).
[21]H. Sickinger, A. Lipman, M. Weides, R. G. Mints, H. Kohlstedt, D. Koelle, R. Kleiner, and E. Goldobin, Phys. Rev. Lett. **109**, 107002 (2012).
[22]S. V. Bakurskiy, N. V. Klenov, T. Yu. Karminskaya, M. Yu. Kupriyanov, and A. A. Golubov, Supercond. Sci. Technol. **26**, 015005 (2013).
[23]D. M. Heim, N. G. Pugach, M. Yu. Kupriyanov, E. Goldobin, D. Koelle, and R. Kleiner, J. Phys.: Condens. Matter **25**, 215701 (2013).
[24]M. Alidoust and J. Linder, Phys. Rev. B **87**, 060503 (2013).
[25]Jun-Feng Liu, K. S. Chan, Phys. Rev. B **82**, 184533 (2010).
[26]V. V. Ryazanov, V. A. Oboznov, A. Yu. Rusanov, A. V. Veretennikov, A. A. Golubov, and J. Aarts, Phys. Rev. Lett. **86**, 2427 (2001).
[27]V. A. Oboznov, V. V. Bol'ginov, A. K. Feofanov, V. V. Ryazanov, and A. I. Buzdin, Phys. Rev. Lett. **96**, 197003 (2006).
[28]T. Kontos, M. Aprili, J. Lesueur, F. Genet, B. Stephanidis, and R. Boursier, Phys. Rev. Lett. **89**, 137007 (2002).
[29]M. Weides, M. Kemmler, H. Kohlstedt, A. Buzdin, E. Goldobin, D. Koelle, and R. Kleiner, Appl. Phys. Lett. **89**, 122511 (2006).
[30]M. Weides, M. Kemmler, H. Kohlstedt, R. Waser, D. Koelle, R. Kleiner, and E. Goldobin, Phys. Rev. Lett. **97**, 247001 (2006).
[31]F. Born, M. Siegel, E. K. Hollmann, H. Braak, A. A. Golubov, D. Yu. Gusakova, and M. Yu. Kupriyanov, Phys. Rev. B **74**, 140501 (2006).
[32]J. Pfeiffer, M. Kemmler, D. Koelle, R. Kleiner, E. Goldobin, M. Weides, A. K. Feofanov, J. Lisenfeld, and A. V. Ustinov, Phys. Rev. B **77**, 214506 (2008).
[33]A. S. Vasenko, A. A. Golubov, M. Yu. Kupriyanov, and M. Weides, Phys. Rev. B **77**, 134507 (2008).
[34]A. S. Vasenko, S. Kawabata, A. A. Golubov, M. Yu. Kupriyanov, C. Lacroix, F. S. Bergeret, and F. W. J. Hekking, Phys. Rev. B **84**, 024524 (2011).
[35]K. D. Usadel, Phys. Rev. Lett. **25**, 507 (1970).
[36]M. Yu. Kuprianov and V. F. Lukichev, Zh. Eksp. Teor. Fiz. **94**, 139 (1988) [Sov. Phys. JETP **67**, 1163 (1988)].
[37]Z. G. Ivanov, M. Yu. Kupriyanov, K. K. Likharev, S. V. Meriakri, and O. V. Snigirev, Fiz. Nizk. Temp. **7**, 560 (1981) [Sov. J. Low Temp. Phys. **7**, 274 (1981)].
[38]A. A. Zubkov, and M. Yu. Kupriyanov, Fiz. Nizk. Temp. **9**, 548 (1983) [Sov. J. Low Temp. Phys. **9**, 279 (1983)].
[39]M. Yu. Kupriyanov, Pis'ma Zh. Eksp. Teor. Fiz. **56**, 414 (1992) [JETP Lett. **56**, 399 (1992)].
[40]A. A. Golubov and M. Y. Kupriyanov, Pis'ma Zh. Eksp. Teor. Fiz. **81**, 419 (2005) [JETP Lett. **81**, 335 (2005)].
[41]A. A. Golubov, M. Y. Kupriyanov, and Y. V. Fominov, Pis'ma Zh. Eksp. Teor. Fiz. **75**, 709 (2002) [JETP Lett. **75**, 588 (2002)].
[42]R. Meservey and P. M. Tedrow, Phys. Rep. **238**, 173 (1994).
[43]E. A. Koshina and V. N. Krivoruchko, Metallofiz. Nov. Tekhnol. **35**, 45 (2013).
[44]L. S. Uspenskaya, A. L. Rakhmanov, L. A. Dorosinskiy, A. A. Chugunov, V. S. Stolyarov, O. V. Skryabina, and S. V. Egorov, Pis'ma Zh. Eksp. Teor. Fiz. **97**, 176 (2013) [JETP Lett. **97**, 155 (2013)].
[45]F. S. Bergeret, A. F. Volkov, and K. B. Efetov, Phys. Rev. Lett. **86**, 3140 (2001).
[46]Ya. V. Fominov, N. M. Chtchelkatchev, and A. A. Golubov, Phys. Rev. B **66**, 014507 (2002).
[47]T. Yu. Karminskaya and M. Yu. Kupriyanov, Pis'ma Zh. Eksp. Teor. Fiz. **85**, 343 (2007) [JETP Lett. **85**, 286 (2007)].
[48]T. E. Golikova, F. Hübler, D. Beckmann, I. E. Batov, T. Yu. Karminskaya, M. Yu. Kupriyanov, A. A. Golubov and V. V. Ryazanov, Phys. Rev. B **86**, 064416 (2012).